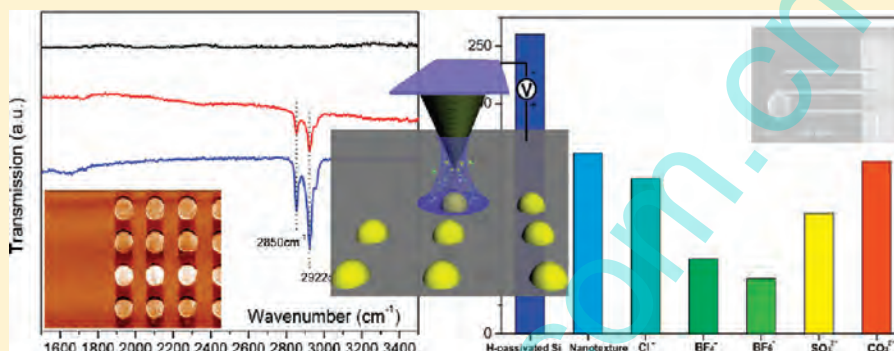


# Fabrication and Adhesion Measurement of a Nanotextured Surface with Ionic Liquid Monolayers

Yufei Mo,<sup>†,‡,\*</sup> Fuchuan Huang,<sup>†</sup> Shulin Pan,<sup>†</sup> and Shizhao Huang<sup>†</sup><sup>†</sup>School of Chemistry & Chemical Engineering, Guangxi University, Nanning 530004, P. R. China<sup>‡</sup>School of Engineering & Applied Science, The George Washington University, Washington, D.C. 20052, United States**ABSTRACT:**

A new approach is presented to fabricate an adhesion-controlled surface by means of local anodic oxide (LAO) lithography combined with ion exchange of ionic liquid. In this research, the nanometer-sized textures are first fabricated using a conductive atomic force microscopy based local anodic oxide method. Ionic liquid molecules were then self-assembled onto the matrix layer of silicon dioxide texture. The adhesive force of the surface was controlled by the formation of a self-assembled monolayer modified texture and ion exchange on the surface. Furthermore, adhesive characterization of ionic liquid and texture layers was investigated with a colloidal probe method. This approach can be readily extended to other conductive substrates, which have potential applications in the fields of detecting or sensing.

## 1. INTRODUCTION

Functional surfaces have been extensively studied because of their great utility in applications ranging from lithography to bioanalysis.<sup>1–3</sup> Functional surfaces with nanohierarchical structure have attracted the increasing interest of researchers from materials science and nanoscience in applications such as hydrophobic,<sup>4,5</sup> virus detection,<sup>6</sup> antiadhesion,<sup>7</sup> and microfluid,<sup>8,9</sup> etc. At present, there is a wide spectrum of technological approaches capable of producing nanostructures. Patterns with dimension of 100 nm or larger have been fabricated using microcontact printing,<sup>10</sup> photolithography,<sup>11</sup> microwriting,<sup>12</sup> and micromachining.<sup>13</sup> However, none of them can be a consideration as an ideal and generally acceptable tool. Ion and electron beam lithography have produced patterns within the films with dimensions of tens of nanometers under ultrahigh vacuum conditions.<sup>14,15</sup> Scanning probe lithography, nanoparticle masks, and nanografting have produced patterns with dimensions of several nanometers within the self-assembled monolayer.<sup>16–18</sup> The nanopattern monolayer produced via scanning probe lithography or nanografting has primarily been negative patterns or in solution.<sup>19–21</sup> The challenging task remains to produce more nanometer or molecular scale structures with a precisely controlled method.

Atomic force microscopes (AFM) enjoy a prominent status in nanotechnology because of their ability to image, at sub-10 nm resolution, a wide variety of surfaces ranging from microchips to

biomolecules. Furthermore, the performance of the instrument is not compromised by the medium. High-resolution imaging has been achieved in vacuum, air, and liquid. The relative ease of conversion of a force microscope into a modification tool has prompted a fascinating variety of atomic and nanometer-scale modification approaches. Those approaches involve the interaction of a sharp probe with a local region of the sample surface. Mechanical, thermal, electrostatic, and chemical interactions, or several combinations among them, are currently exploited to modify surfaces at the nanoscale with probe microscopes. AFM-based nanolithography has wide applications in nanoscale patterning and fabrication. So far, dip-pen,<sup>22,23</sup> local oxidation,<sup>24</sup> and other techniques<sup>25–27</sup> have been developed to selectively modify a surface and build up complex nanostructures.

In AFM local anodic oxidation (LAO), the negatively biased tip induces simultaneous oxide growth on conductive surfaces. It is suggested that the oxidation mechanism and kinetics are closely related to electrical field, surface stress, water meniscus, and OH-diffusion, etc.<sup>28–31</sup> Ultrathin oxide patterns, thickness  $\leq 5.0$  nm, have been fabricated on a silicon surface using AFM

**Received:** February 8, 2011**Revised:** April 3, 2011**Published:** May 02, 2011

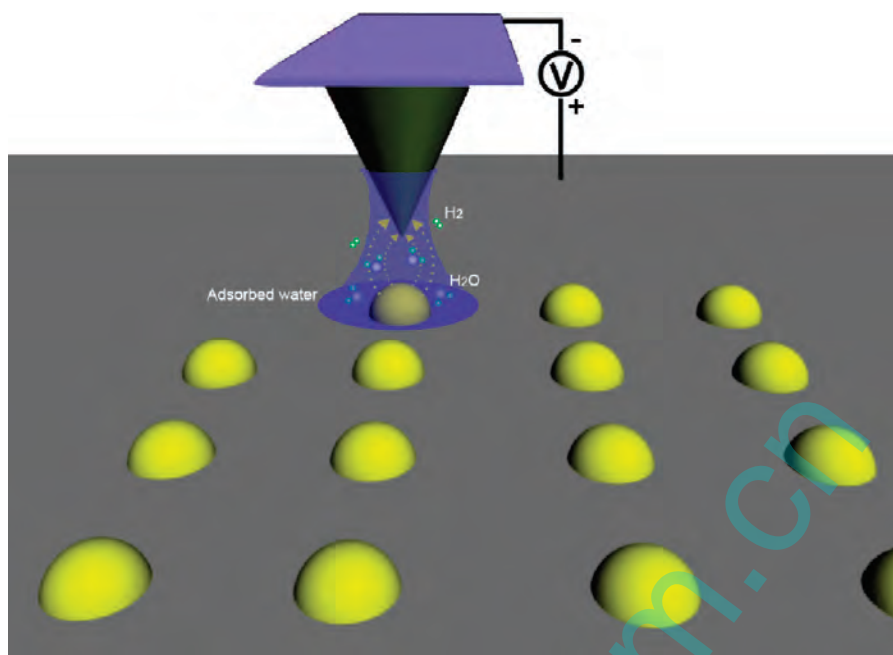


**Figure 1.** Schematics of the chemical reactions in AFM local electric field induced oxidation.

oxidation.<sup>32,33</sup> Besides being a powerful fabrication tool to grow oxide, AFM is also a good technique to measure adhesive forces and friction between surfaces in the nanometer scale. Adhesive forces come from two sources: contact interfacial forces and noncontact forces such as van der Waals or electrostatic forces. Adhesion is typically measured by pull-off forces between the cantilever tip and the surface. The challenge in the measurement often lies with the determination of real area of contact. For sharp tips, the surface roughness and high contact pressure may cause the tip to rotate and the surface to deform. Ducker<sup>34</sup> introduced the used of colloidal probe tips by attaching a sphere to the cantilever to measure adhesion. The spherical shape of the AFM tip provides controlled contact pressure, symmetry, and mostly elastic contacts. For AFM-LAO adhesion measurement of nanotextures, the spherical probe tip can fully contact with the texture surface, while the sharp tip can only point contact. However, the measurement of the contact surface roughness of a colloidal probe poses additional challenges since the total surface areas are very small. Therefore, the reverse AFM imaging method which is developed by Neto<sup>35</sup> was adopted to identify the contact location and directly imaged by an AFM with a sharp tip to provide detailed three-dimensional surface topography.

In this paper, a combined system consisting of nanotexture and self-assembled monolayer was designed for adhesion control. In our approach, silicon surfaces were micropatterned by the AFM-LAO process after H-passivity. The patterned surfaces were modified with an ionic liquid self-assembled monolayer for lowering surface energy. In our previous research,<sup>36</sup> the LAO process is well controlled by several major parameters as follows: pulse bias voltage, pulse width, writing speed, and humidity. The desired dimension of the predesigned nanostructure can be fabricated by controlling these parameters. The adhesion and nanostructure produced in each step are also characterized using AFM. The aim of this work was to further improve the knowledge of the relations between the micropattern, surface chemistry, and nanotribological properties. It is expected that this

investigation could help to understand and aid the design and selection of the appropriate SAM–texture system for protection in nanodevices.

## 2. EXPERIMENTAL SECTION

Experiments were performed on p-doped single-side polished single-crystal silicon (100) substrates with a resistivity  $<0.005\Omega$  (Benyuan Technology Co. Ltd., Beijing). After ultrasonic cleaning by acetone and isopropanol in turn, Si substrates were placed into an ultrahigh vacuum (UHV) chamber at a base pressure of  $5 \times 10^{-11}$  Torr for a hydrogen passivated process. Atomic H was created by cracking  $H_2$  molecules on a  $1500^\circ\text{C}$  tungsten filament, and the Si substrates were passivated by atomic H in the UHV chamber. The advantages of the H-passivated process are to prevent nonuniform native oxidation and improve resolution of Si oxide nanotextures.

The AFM platform is a commercial environment-controlled CSPM 4000 multimode system. A conductive platinum covered probe (Budget sensor) is used in the local oxidation process. The tip is conic with radius below 25 nm. The AFM software was extended with a program package for well-defined movement of the tip over a sample. Relative humidity was controlled by inducing a mixture of dry and moist nitrogen stream inside the AFM chamber, while the temperature was maintained at  $25 \pm 2^\circ\text{C}$ . The oxidation process is sensitive to many parameters: dc pulse voltage, pulse widths, writing speed, and relative humidity. The AFM-LAO process is schematically shown in Figure 1. In this technique, oxides grow on a chemically reactive substrate by the application of a voltage between a conductive AFM tip and a substrate surface which acts as an anode. There is a threshold voltage at which the anodic oxidation starts. Water molecules adsorbed on a substrate dissociate due to a high electric field ( $E > 10^7\text{ V/m}$ ),<sup>37</sup> into fragments ( $H^+$ ,  $OH^-$ , and  $O^{2-}$ ), and act as an electrolyte. Oxygen-containing radicals then contribute to the formation of oxides and, due to an electric field-enhanced diffusion through the Si oxide layer, also to the growth of the Si oxide underneath.

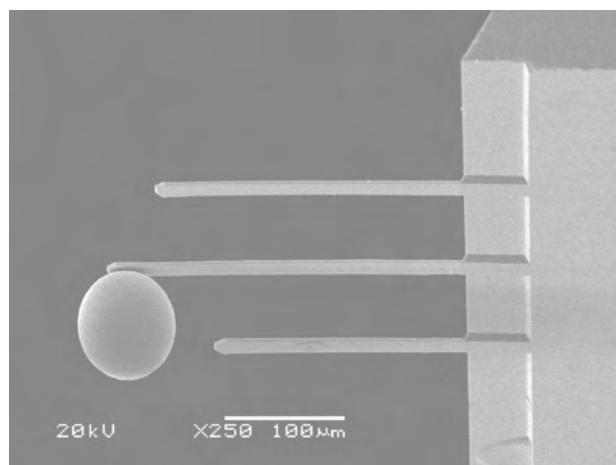


**Figure 2.** Image of a typical colloidal probe obtained from the SEM microscope.

Ge attenuated total reflectance Fourier transform infrared (GATR-FTIR) spectra were recorded on a Bruker IFS 66 V/S Fourier transformation infrared spectrometer. The spectra of the sample were obtained using a Harrick Scientific horizontal reflection GATR accessory ( $65^\circ$  incidence angle). The samples were placed in contact with the flat surface of a semispherical Ge crystal which serves as the optical element. The spectra were collected for 32 scans with resolution of  $4\text{ cm}^{-1}$ . The background was collected using the accessory with no sample placed on it. To eliminate the effect of  $\text{H}_2\text{O}$  and  $\text{CO}_2$ , the pressure in the sample chamber and optical chamber was kept below  $6.0 \times 10^{-4}$  MPa.

Molecular composition and structure of the surface were examined with a PHI-5702 multitechnique X-ray photoelectron spectrometer (XPS), using a pass energy of 29.35 eV, an excitation source of Mg K $\alpha$  radiation ( $h\nu = 1253.6\text{ eV}$ ), and a takeoff angle of  $36^\circ$ . The chamber pressure was about  $3 \times 10^{-8}$  Torr during testing. Peak deconvolution and quantification of elements were accomplished using the software and sensitivity factors supplied by the manufacturer. The binding energy of adventitious carbon (C1s: 284.8 eV) was used as a reference.

Colloidal probes were prepared by gluing glass spheres of radius of  $50\ \mu\text{m}$  onto individual tipless cantilevers (Budget sensor), as shown in Figure 2. The colloidal probes were cleaned by high-purity ethanol in an ultrasonic bath for 1 min and then in a plasma cleaner for 30 s. Before use, the force constant of each probe was calibrated using individually measured thickness, width, and length, which are determined by a scanning electron microscope.<sup>38</sup> To scan only the contact area of the probe, a specially designed holder was fabricated to hold the colloidal probe at a specific inclined angle, and the contact surface was scanned. The surface topographies of the colloidal probes were scanned with a  $0.12\text{ N/m}$   $\text{Si}_3\text{N}_4$  cantilever and sharp tip under contact mode. The force constant and root-mean-square roughness of the colloidal probe were estimated to be  $0.35\text{ N/m}$  and  $0.2\text{ nm}$ , respectively. For all measurements, the same cantilever was used in this comparative study. Furthermore, to avoid influence of molecules which may transfer to the tip on the AFM/FFM experiments, the tip was scanned on a cleaved mica surface to remove these physical adsorbed molecules. During adhesion measurement, the laser beam is focused on the back of the AFM cantilever to detect the cantilever's deflection as it interacts with the surface beneath it. The reflected beam is

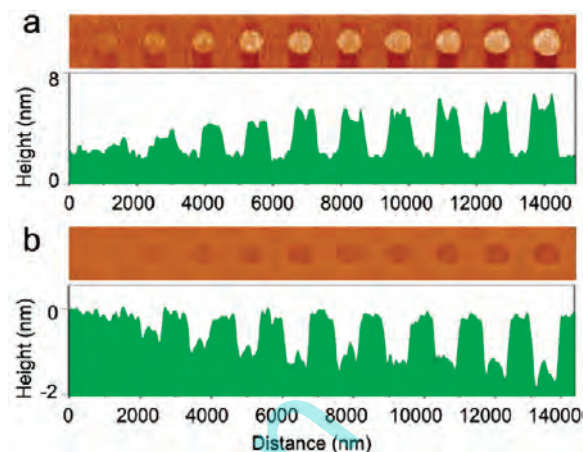


**Figure 3.** Testing line of Si oxide pillars prepared at different bias voltages and pulsewidths (a) and nanoholes obtained by selective etching of these pillars in 1% HF (b).

directed onto a split photodiode detector, which produces a voltage signal proportional to the cantilever deflection. The sample beneath the cantilever is moved using a piezoelectric transducer. In the force measurements, motions in the  $x$  and  $y$  directions are disabled; the piezoelectric tube is used to move the surface in the  $z$  direction; and the cantilever deflection is continuously measured. The surface is first moved toward the cantilever until the tip contacts the surface and then is retracted from the cantilever until the tip snaps off from the surface. The adhesion force was obtained from measuring the deflection of the cantilever at the point where the tip pulls off from the surface after contact. In this research, at least 200 different measuring locations were carried out for each scan range, and also at least 10 consecutive adhesion force measurements in each location were taken and averaged. The relative humidity was controlled at 20% RH. Repeated measurements were within 5% of the average value for each sample.

### 3. RESULTS AND DISCUSSION

**3.1. Structure and Morphology Characterization of Nanostructures.** Fabrication of nanostructures for a study of their unique quantum properties requires a reliable control of individual technological steps. To be able to prepare nanostructures of required dimensions and properties, the relations between the operation parameters of fabrication and the resultant product parameters should be fairly well-known and understood. The LAO process is controlled by several major parameters as follows: writing speed, pulse bias voltage, pulse widths, and humidity. Figure 3a shows a testing line of Si oxide pillars that was prepared at controlled tip–sample voltages and pulse widths. On the surface, the pillars with the average diameter about  $700\text{ nm}$  are arranged, and the distance between the adjacent pillars is about  $600\text{ nm}$  in this dimension. From right to left, the pillars were made at progressively decreasing pulse bias voltages and pulse widths. The height of the pillars ranges from  $0.8$  to  $6.4\text{ nm}$ , as shown in the cursor profile of the figure. It is obvious that the pillar was prepared at the higher pulse voltage, and the longer pulsewidth is the best developed one in height. Such a testing pillar array makes it possible to find the relation between the height of the nanostructure and operational parameters. As shown in Figure 3b, the Si negative pattern was

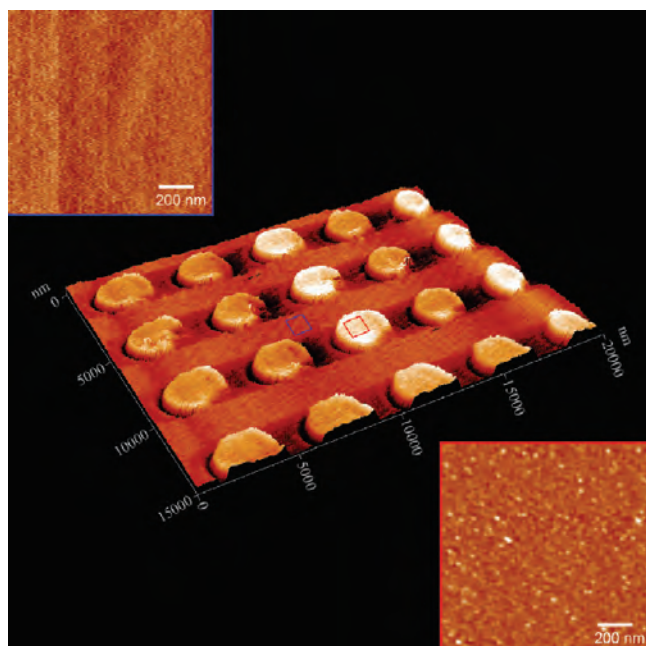


**Figure 4.** AFM topographic image of IL SAM modified patterned H-passivated Si. Insets correspond to the selected rectangle area.

fabricated by selective etching of Si oxide pillars in 1% HF solution. The cursor profile of this figure reveals that the height of nanoholes is about 0.5–1.8 nm. Results indicate that this process can be used not only to fabricate a positive pattern but also to prepare a negative patterning of substrates and thin films.

**3.2. Characterization of the Films.** 1-Alkyl-3-(3-triethoxysilypropyl) imidazolium chloride ( $[C_n\text{AIM}]\text{Cl}$ ) was synthesized by a similar method<sup>39</sup> ( $[C_n\text{AIM}]\text{Cl}$ ,  $n = 1, 8$ ) and was treated with either  $\text{NaBF}_4$  or  $\text{NaPF}_6$  in acetonitrile to yield  $[C_n\text{AIM}]\text{BF}_4$  or  $[C_n\text{AIM}]\text{PF}_6$ , respectively. The IL SAMs were formed by immersing freshly patterned silicon substrates in 1% (W/V) toluene solution of ILs and heating to reflux at 120 °C for 24 h. The thickness of  $[C_n\text{AIM}]_x$  SAMs was performed on a L-116-E ellipsometer. The ellipsometric thicknesses were 0.5 nm for SAM of  $[C_1\text{AIM}]\text{BF}_4$  and 1.2 nm for  $[C_8\text{AIM}]\text{BF}_4$ , respectively. In this study, IL SAMs were formed with various anions on the surface by ion exchange. For the exchange of anions, the  $[C_n\text{AIM}]\text{Cl}$  self-assembled onto the substrate. Then, the substrate with the IL SAM of  $[C_n\text{AIM}]\text{Cl}$  was immersed in an aqueous 5 mM solution of  $\text{NaBF}_4$  or  $\text{NaPF}_6$  without stirring at room temperature for 12 h and then rinsed extensively with  $\text{H}_2\text{O}$  followed by ethanol and dried under a nitrogen stream. The three-dimensional surface topography of the IL-modified pattern was shown in Figure 4. To observe these pillars in more detail, the scanning area was narrowed. The insets of this figure show the AFM topography of the selected rectangle region. The unoxidized H-passivated Si surface was shown in the upper inset. The lower inset shows the image of the textured surface. The results indicate that the  $[C_n\text{AIM}]\text{Cl}$  ionic liquid is more prone to adsorb onto the surface of silicon oxide after self-assembled and rinsing processes.

The successful grafting of  $[C_n\text{AIM}]\text{Cl}$  ionic liquid onto patterned silicon surfaces was also confirmed by means of GATR-FTIR spectroscopy. The GATR-FTIR spectra of the  $[C_n\text{AIM}]\text{Cl}$  ionic liquid on a textured silicon surface is shown in Figure 5. The vibrational signatures of methylene in the films appear at 2850 and 2922  $\text{cm}^{-1}$ , assigned to symmetric and asymmetric vibrations, respectively. According to the previous report,<sup>40,41</sup> the symmetric

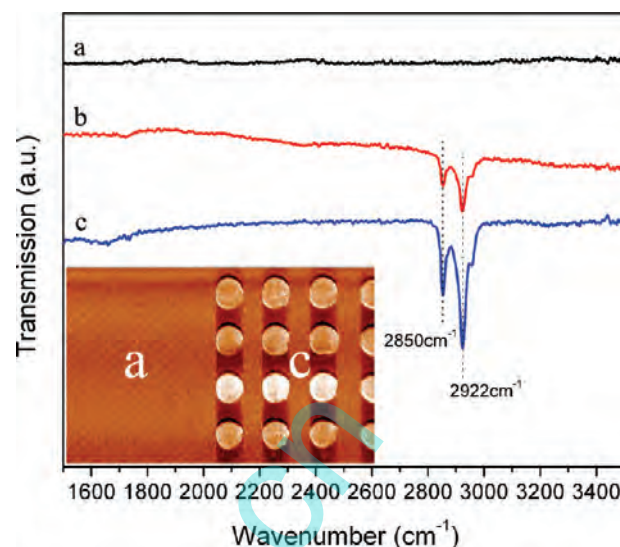


**Figure 5.** FTIR spectra of IL films on H-passivated Si with and without LAO texture ( $[C_n\text{AIM}]\text{Cl}$ ,  $n = 1, 8$  corresponding to b, c).

and asymmetric methylene vibrations typically appear in the range of 2846–2850 and 2915–2918  $\text{cm}^{-1}$  for liquid-like disordered chains. Furthermore, the change of anions on the surface was confirmed by XPS. In this process, the anion was chosen to exchange from  $\text{Cl}^-$ ,  $\text{BF}_4^-$ , to  $\text{PF}_6^-$ . Figure 6a shows the XPS survey spectra of the IL film at the main exchange process of anions. The XPS survey spectra exhibit seven elements: silicon (Si 1s, Si 2p) carbon (C 1s), oxygen (O 1s), nitrogen (N 1s), fluorine (F 1s), boron (B 1s), and chlorine (Cl 2p). A peak of 198.4 eV can be assigned to the Cl atom in the curve of  $[C_8\text{AIM}]\text{Cl}$ , and no peaks related to Cl species appear in the curves of  $[C_8\text{AIM}]\text{BF}_4$  and  $[C_8\text{AIM}]\text{PF}_6$ . It means that the  $\text{Cl}^-$  anions were removed completely after the exchange process of anions. While the peak appearing at 193.5 eV is assigned to the B atom in the  $\text{BF}_4$  anion (Figure 6b), the peak that appeared at 136.5 eV can be attributed to the P atom in the  $\text{PF}_6$  anion (Figure 6c).

**3.3. Adhesion Measurement.** Adhesive force measurements were performed in a noise- and vibration-isolated and environment-controlled friction force microscope. Adhesion is generally measured by the amount of force necessary to separate two surfaces in contact. At nanoscale, mechanical loading is often not the overwhelming force as in the macroscale, and surface forces such as van der Waals, electronic, and capillary force become significant in controlling pull-off force. As seen in Figure 7, the adhesive forces are closely related to surface nanotextures and also are strongly influenced by chemical modification with ionic liquid SAMs. Strong adhesive force is observed on the bare H-passivated Si surface, on which the adhesive force is as high as about 260 nN. Once the nanotextures were fabricated on H-passivated Si surface, the adhesive force was greatly decreased to 157 nN. After  $[C_8\text{AIM}]\text{Cl}$  ionic liquid modification, the adhesive force further decreased to 135 nN. Furthermore, the adhesion of the surface was examined after ion exchange. As shown in this figure, all of the anion-substituted ionic liquid SAMs showed lower adhesive forces than that of  $[C_8\text{AIM}]\text{X}$  having a Cl anion. Among them, the  $[C_8\text{AIM}]\text{X}$  having the  $\text{PF}_6^-$  anion exhibited the lowest adhesive force of 58 nN. It is also observed that the  $[C_8\text{AIM}]\text{BF}_4$  bearing fluorinated anions displayed lower adhesive force than those having other anions, such

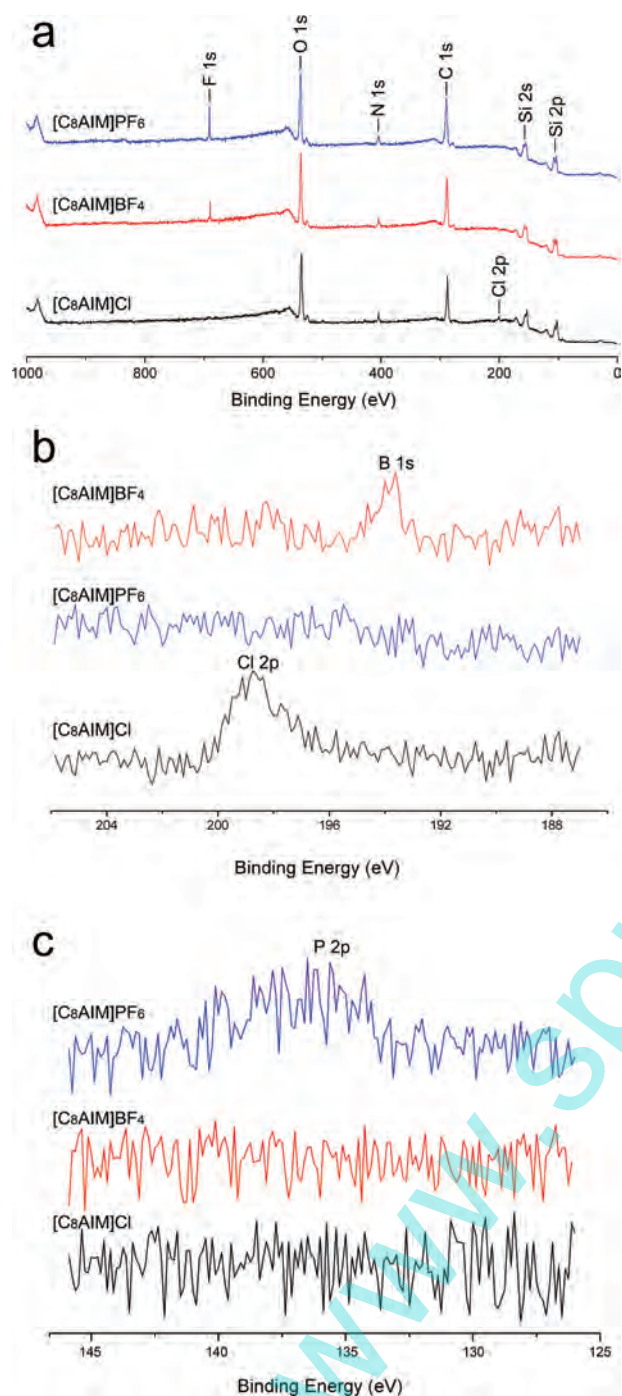


**Figure 6.** X-ray photoelectron spectra of surfaces presenting  $[\text{C}_8\text{AIM}]\text{Cl}$ ,  $[\text{C}_8\text{AIM}]\text{BF}_4$ , and  $[\text{C}_8\text{AIM}]\text{PF}_6$ . (a) Survey spectra of IL SAM textured surface. (b) High-resolution spectra between 186 and 206 eV, and peaks of B 1s and Cl 2p were observed in the spectra. (c) High resolution spectra between 125 eV and 147 eV, and a peak of P 2p was observed in the spectra.

as  $\text{CO}_3^{2-}$  and  $\text{SO}_3^{2-}$ . The result is probably due to hydrophilic properties of the anionic groups with  $\text{CO}_3^{2-}$  and  $\text{SO}_3^{2-}$  in the upper of the IL layer which facilitates the formation of a meniscus between the probe and surface, which increases the adhesive force. The adhesive force is lower in  $[\text{C}_8\text{AIM}]\text{X}$  bearing fluorinated anions since they have the greatest amount of relative hydrophobic anionic groups to decrease the tip–sample adhesion. The changes

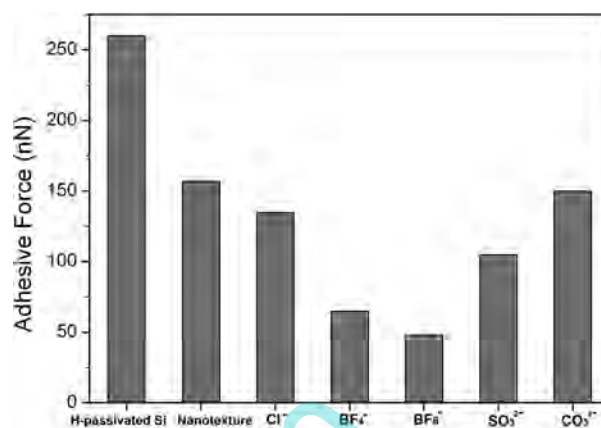


**Figure 7.** Plots of adhesive forces between the AFM colloidal probe and the surfaces before and after ion exchange.

in the adhesive force clearly show that surface force could be controlled by changes in counteranions of imidazolium ions.

#### 4. CONCLUSIONS

In this study, a simple and versatile approach is reported for fabricating an adhesion-controlled surface by combining local anodic oxide, self-assembly, and ion exchange. The functionalized imidazolium ionic liquids were designed and synthesized with the aim of controlling the adhesive force of the textured surface. The effect of nanotexture and surface ion exchange on the adhesion of surfaces was investigated systematically. The results indicate that adhesive force could be evidently induced by designing a suitable surface texture combined with a hydrophobic anion modified on the surface. We believe that the anion effect on surface force is of general significance to the adsorption on patterned surfaces. This effect could be advantageously incorporated in the applications of monolayer-based technologies such as antiadhesion, anion sensor, microfluidics, and nanodevices.

#### AUTHOR INFORMATION

##### Corresponding Author

\*E-mail: yufeimo@gxu.edu.cn.

#### ACKNOWLEDGMENT

This work was funded by the National Natural Science Foundation of China (NSFC) under grant No. 20773148 and the Scientific Research Foundation of Guangxi University (Grant No. XBZ100118).

#### REFERENCES

- (1) Yu, B.; Dong, H.; Qian, L.; Chen, Y.; Yu, J.; Zhou, Z. *Nanotechnology* **2009**, *20*, 465303.
- (2) Baserga, A.; Vigano, M.; Casari, C. S.; Turri, S.; Bassi, A. L.; Levi, M.; Bottani, C. E. *Langmuir* **2008**, *24*, 13212.
- (3) Kobayashi, K.; Tonegawa, N.; Fuji, S.; Hikida, J.; Nozoye, H.; Tsutsui, K.; Wada, Y.; Chikira, M.; Haga, M. *Langmuir* **2008**, *24*, 13203.
- (4) Aulin, C.; Yun, S.; Wågberg, L.; Lindström, T. *ACS Appl. Mater. Interfaces* **2009**, *1*, 2443.
- (5) Narhe, R. D.; Beysens, D. A. *Langmuir* **2007**, *23*, 6486.
- (6) Alsteens, D.; Pesavento, E.; Chevart, G.; Dupres, V.; Trabelsi, H.; Soumilion, P.; Dufrene, Y. F. *ACS Nano* **2009**, *3*, 3063.
- (7) Mo, Y.; Wang, Y.; Pu, J.; Bai, M. *Langmuir* **2009**, *25*, 40.

- (8) Ell, J.; Crosby, T. A.; Peterson, J. J.; Carter, K. R.; Watkins, J. J. *Chem. Mater.* **2010**, *22*, 1445.
- (9) Fang, X.; Liu, Y.; Kong, J.; Jiang, X. *Anal. Chem.* **2010**, *82*, 3002.
- (10) Husemann, M.; Mecerreyes, D.; Hawker, C. J.; Hedrick, J. L.; Shah, R.; Abbott, N. L. *Angew. Chem., Int. Ed.* **1999**, *38*, 647.
- (11) Tarlov, M. J.; Burgess, D. R.F.; Gillen, G. J. *Am. Chem. Soc.* **1993**, *115*, 5305.
- (12) Abbott, N. L.; Kumar, A.; Whitesides, G. M. *Chem. Mater.* **1994**, *6*, 596.
- (13) Abbott, N. L.; Folkers, J. P.; Whitesides, G. M. *Science* **1992**, *257*, 1380.
- (14) Berggren, K. K.; Bard, A.; Wilbur, J. L.; Gillaspay, J. D.; Helg, A. G.; McClelland, J. J.; Rolston, S. L.; Phillips, W. D.; Prentiss, M.; Whitesides, G. M. *Science* **1995**, *269*, 1255.
- (15) Sondag-Huethorset, J. A. M.; Van Helleputte, H. R. J.; Fokkink, L. G. J. *Appl. Phys. Lett.* **1994**, *64*, 285.
- (16) Ross, C. B.; Sun, L.; Crook, R. M. *Langmuir* **1993**, *9*, 632.
- (17) Piner, R. D.; Zhu, J.; Xu, F.; Hong, S. H.; Mirkin, C. A. *Science* **1999**, *283*, 661.
- (18) Mo, Y. F.; Bai, M. W. *J. Phys. Chem. C* **2008**, *112*, 11257.
- (19) Xiao, D.; Liu, G. Y.; Charych, D. H.; Salmeron, M. *Langmuir* **1995**, *11*, 1600.
- (20) Xu, S.; Miller, S.; Laibinis, P. E.; Liu, G. Y. *Langmuir* **1999**, *15*, 7244.
- (21) Wadu-Mesthrige, K.; Xu, S.; Amro, N. A.; Liu, G. Y. *Langmuir* **1999**, *15*, 8580.
- (22) Piner, R. D.; Zhu, J.; Xu, F.; Hong, S.; Mirkin, C. A. *Science* **1999**, *283*, 661.
- (23) Hong, S.; Zhu, J.; Mirkin, C. A. *Science* **1999**, *286*, 523.
- (24) Mo, Y. F.; Wang, Y.; Bai, M. W. *Phys. E* **2008**, *41*, 146.
- (25) Wacaser, B. A.; Maughan, M. J.; Mowat, I. A.; Niederhauser, T. L.; Linford, M. R.; Davis, R. C. *Appl. Phys. Lett.* **2003**, *82*, 808.
- (26) Lee, H.; Kim, S. A.; Ahn, S. J.; Lee, H. *Appl. Phys. Lett.* **2002**, *81*, 138.
- (27) Ahn, S. J.; Jang, Y. K.; Lee, H.; Lee, H. *Appl. Phys. Lett.* **2002**, *80*, 2592.
- (28) Lazzarino, M.; Padovani, M.; Mori, G.; Sorba, L.; Fanetti, M.; Sancrotti, M. *Chem. Phys. Lett.* **2005**, *402*, 155.
- (29) Lazzarino, M.; Mori, G.; Sorba, L.; Ercolani, D.; Biasiol, G.; Heun, S.; Locatelli, A. *Surf. Sci.* **2006**, *600*, 3739.
- (30) Garcia, R.; Martinez, R.; Martinez, V. J. *Chem. Soc. Rev.* **2006**, *35*, 29.
- (31) Patermarakis, G. S.; Kytopoulos, V. N. *Mater. Lett.* **2007**, *61*, 4997.
- (32) Dagata, J. A.; Perez-Murano, F.; Abadal, G.; Morimoto, K.; Inoue, T.; Itoh, J.; Yokoyama, H. *Appl. Phys. Lett.* **2000**, *76*, 2710.
- (33) Blasco, X.; Nafria, M.; Aymerich, X. *Surf. Sci.* **2003**, *732*, 532.
- (34) Ducker, W. A.; Senden, T. J.; Pashley, R. M. *Nature* **1991**, *353*, 239.
- (35) Neto, C.; Craig, V. S. J. *Langmuir* **2001**, *17*, 2097.
- (36) Mo, Y.; Zhao, W.; Wang, Y.; Zhao, F.; Bai, M. *Ultramicroscopy* **2009**, *109*, 247.
- (37) Jian, S. R.; Fang, T. H.; Chuu, D. S. *J. Phys. D: Appl. Phys.* **2005**, *38*, 2432.
- (38) Liu, Y. H.; Wu, T.; Evans, D. F. *Langmuir* **1994**, *10*, 2241.
- (39) Mehnert, C. P.; Cook, R. A.; Dispenziere, N. C.; Afeworki, M. *J. Am. Chem. Soc.* **2002**, *124*, 12932.
- (40) Zhang, Q.; Archer, L. A. *J. Langmuir* **2005**, *21*, 5405.
- (41) Zhang, Q.; Archer, L. A. *J. Phys. Chem. B* **2003**, *107*, 13123.